Ballistically emplaced impact melt around the lunar crater Pierazzo

Veronica Bray[1], Corwin Atwood-Stone[1], Catherine D. Neish[2,3], Natalia Artemieva[4,5], Alfred McEwen[1], Jim N. McElwaine[4,6]

[1]Lunar and Planetary Laboratory, University of Arizona, Tucson, AZ 85721, USA

[2]Department of Earth Sciences, The University of Western Ontario, London, Canada

[3]Centre for Planetary Science and Exploration, The University of Western Ontario, London, Canada

[4]Planetary Science Institute, Tucson, AZ 85791, USA

[5]Institute for Dynamics of Geospheres, Moscow, Russia

[6]Department of Earth Sciences, University of Durham, Durham, UK

Abstract

Impact melt flows are observed to emerge from the continuous and discontinuous ejecta blanket of the 9 km lunar crater Pierazzo, from the crater rim to more than 40 km away from the center of the crater. Our mapping and modeling results suggest that melt can be incorporated into ejecta and emplaced ballistically. It also confirms the idea that impact melt can travel beyond the continuous ejecta blanket.. Our analysis is based on the identification of established melt morphology for these in-ejecta flows, and their occurrence on 6 to 18° slopes - too shallow for dry granular flows beginning at rest. We also compared the fractal dimension of the flow boundaries to established melt and granular flows, providing more support for these flows being melt-rich instead of granular in origin.

Ejected melt flows are noted within just 1.5% of the mapping area, suggesting that the surface expression of impact melt in the extended ejecta around craters of this size is rare. We hypothesize that a mix of solid and molten ejecta impacts the ground together and continues to travel across the surrounding terrain at speeds high enough to maintain turbulent mixing. This quickly quenches the melt present, preventing most coherent melt pockets from settling out within the majority of the extended ejecta deposit, unless the melt 'pocket' is especially large. As most of the flows mapped in this work occur on crater-facing slopes, the development of defined melt flows within ejecta deposits might be facilitated by influence of high crater-facing topography to stall or impede the ejecta flow soon after it makes ground contact, preventing the continuation of turbulent mixing. These surface expressions of melt within ejecta blankets suggest that melt rock masses can exist within ejecta, creating a heterogeneous deposit.

1. Introduction

One of the primary characteristics of impact crater formation is the generation of melted target rock. Decompression melting of the target rocks occurs during the initial stages of impact, after passage of the impact shock wave [e.g., *Dence et al*., 1977]. Although difficult to estimate, the majority of impact melt in both simple and complex craters is expected to remain within the crater cavity [e.g. *Kraus et al.*, 2011, after *Maxwell* 1977]. Some melt is ejected and is deposited outside of the crater rim, especially in oblique impacts [e.g., *Chadwick and Schaber* 1993]. Close to the rim, the impact melt lining the transient cavity will be deposited as wall veneers and near-rim melt deposits [e.g., *Hawke and Head*, 1977]. *Osinski et al.* [2011] suggested that an even later-stage of near-rim melt deposition occurs as a result of central uplift movement during the modification stage of complex crater formation, pushing large volumes of melt over the rim of complex craters.

A wide variety of impact melt products have been found on Earth, ranging in distribution from coherent melt deposits within the crater cavity to far-flung glassy ejecta (tektites). They range in composition from pure impact glass to minor/major constituents of impact melt-bearing breccias. In most cases, impact melt deposits outside of the crater rim lie stratigraphically above melt-poor ejecta layers [e.g., *Osinski et al.*, 2011 and references therein]. However, observations of melt ponds around some lunar craters suggest the secondary impact of solid debris into possibly still-molten ponds of impact melt [*Plescia*, 2015; *Zanetti*, 2015; *Zanetti et al.*, 2017], pointing toward an even more intricate interplay between ejecta and melt deposition.

Determining the distribution of melt products in and around impact craters will aid in the understanding of impact induced melting, the excavation stage of impact cratering, and the emplacement processes for both high-shock (melt) and low-shock (rocky debris) materials. Unfortunately for terrestrial studies, the poor preservation state of most impact crater ejecta limits our research of melt outside of impact crater rims [e.g. *Osinski et al*., 2011]. As a result, we turn to planetary bodies with (a) substantial impact melting and (b) limited weathering to study these processes. Surficial impact melts are obvious in and around many fresh lunar craters as relatively low albedo deposits that show evidence of a fluid nature (such as equi-potential surfaces, flow patterns, channels — *e.g.*, *Hawke & Head*, [1977]) followed by cooling and sometimes sustained surface flow [*e.g.*, *Bray et al.*, 2010]. The minimal weathering rate on the Moon allows these melts to be preserved over much longer timescales than those on the Earth, making them an ideal target for the study of impact cratering and melt emplacement.

Recent high-resolution datasets show impact melt in and around lunar craters to be more voluminous, spatially extensive, and mobile over longer time periods than previously thought [*e.g.*, *Bray et al.*, 2010; *Plescia and Cintala*, 2012; *Bandfield et al*., 2013; *Neish et al.,* 2014; *Stopar et al*., 2014]. Most flows studied using these new datasets are near-rim flows that emanate from melt ponds at the crater rim, and melt ponds throughout the continuous ejecta blankets (1–2 crater radii from the rim; c.f. *Melosh*, 1989) [e.g., *Zanetti*, 2015]. As research with high resolution data sets continues, further field examples are becoming more widely noted.

A far-afield example of possible melt-ejection is the Lunar Reconnaissance Orbiter Camera (LROC) imaging of apparent impact melt deposits at the antipode of Tycho crater [*Robinson et al*., 2016]. These areas are also consistent with regions of high rock abundance as observed by the Lunar Reconnaissance Orbiter’s (LRO) Diviner instrument [*Bandfield* *et al.,* 2017]. These melt deposits are generally smooth, dark and ponded (like Figure 1B), are associated with no local fresh craters or volcanic sources and are suggested to originate from source craters at least 250 km distant [*Robinson et al.,* 2016].

Regions of exterior impact melt reaching up to 5.3 crater radii from the crater rims have also been identified using LRO Mini-RF images [*Neish et al.,* 2014], where melt-rich deposits are characterized by particularly high (>1) circular polarization ratios (CPR) [*Carter et al.,* 2012; *Neish et al*., 2014]. Many ejecta blankets are streaked with such high CPR regions, suggesting the possible presence of impact melt-rich deposits in the distal ejecta (>5 crater radii from the crater rim). However, as blocky ejecta also produce high CPR values, this technique cannot be used for melt identification without additional morphologies consistent with melt flows (*i.e.*, lobate margins) being identified within these areas.

If LROC, Diviner and Mini RF identification of far-flung melt deposits are correct, it has implications for the amount of impact melt generated during impacts, the process of ejecta flow during crater excavation, and the impact-derived melt content of the lunar regolith. This paper presents high-resolution mapping of melt ponds and possible melt flows at distances intermediate to the near-rim melts and the distant antipodal melts. Our study region thus falls in the discontinuous ejecta blanket that is unable to be studied for terrestrial craters, where any coherent melt present must have been ejected as part of the excavation flow.

2. Methods

Impact melt emplaced exterior to a crater rim can include both melt ejected as part of the excavation flow and melt pushed over the crater rim during the modification stage of impact crater formation [*Hawke and Head*, 1977; *Osinski et al*. 2011]. Assessment of the former thus requires our study to be based upon simple craters in which minimal modification (rim slumping, central uplift, etc.) has occurred. Although we present data from a range of lunar craters, this work concentrates on the analysis of Pierazzo crater (9.2 km in diameter East-West and 8.6 km North-South), a simple crater located on the far side of the Moon (259.7E, 3.25N). This crater was selected due to extensive LRO Narrow Angle Camera (NAC) coverage. This rayed crater is typical of lunar simple craters of its size [*Pike*, 1976], with a depth-diameter ratio of 0.2 and a wall slope slightly above 30°. The visible ray system from Pierazzo crater extends beyond 450 km from the crater rim and has a slight asymmetry, suggesting a slightly oblique E to W impact. The extensive rays also suggest a relatively young age for Pierazzo, so that any small-scale features in the ejecta blanket should remain in a relatively fresh state.

2.1. Mapping

Ten LRO NAC [*Robinson et al.*, 2010] image pairs of the crater and the surrounding area were mosaicked (Figure 2A) forming a study area of approximately 3300 km^2. The Global Lunar Digital Terrain Model 100m data set (GLD100, *Scholten et al.*, [2012]) was used to provide topographic context for the mapping area. The image mosaic was generated from NACs with pixel scales ranging from ~0.5 m/pixel to ~1.5 m/pixel and normalized to a resolution of 1.5 m/pixel. We mapped the following units on the LRO NAC images: (1) Flow features and ponds (black regions in Figure 2B; examples are shown in Figure 3B and Figures 4 - 6), (2) low albedo blocky ejecta (dark grey regions in Figure 2B) including dark ‘streamers’ (Figure 3A; c.f. *Plescia and Cintala*, [2012]), and (3) low albedo candidate melt deposits (lighter grey regions in Figure 2B). Mapping was performed in ESRI’s ArcMap software and the resulting mapping units are presented in Figure 2B. All measurements recorded relative to the crater center were taken from the mosaic with an associated measurement error of 3 m, based on pixel scale. Additional errors due to uncertainty in the position of the crater center within the mosaic might also exist. Measurements of individual flow lengths, widths and shadow-length derived heights were recorded from individual NACs with an associated error of 1-3m depending on the image resolution. GLD100 topography was added to the analysis after visual mapping had been completed to remove bias in our mapping.

2.2 Assessment of Flow Characteristics

To determine whether some or all of the flows found on the extended ejecta blanket could be impact melt rich, we compared the flow morphology to well-established melt and dry granular flows on the Moon. Morphology and albedo comparisons are presented in a qualitative manner. Figure 1 shows examples of melt deposits within the proximal ejecta blanket (within 5 crater radii of the rim; c.f. *Stöffler and Grieve,* 2007) of Giordano Bruno — a 22km diameter lunar crater with complex morphology (rim slumping, terracing, and floor hummocks). The melt deposits at Giordano are larger than at the 9 km Pierazzo crater, providing clearer (at LROC resolution) examples of the melt textures referred to in this work.

Our assessment of whether flows are melt-rich or melt-poor relies primarily on the presence, or not, of melt textures. As a supporting dataset, we employed fractal analysis as a way to quantitatively compare the observed ejecta flows to other lunar melt-rich and dry granular flows. The margins of basaltic flows on Earth have been found to be fractal [e.g., *Bruno et al*., 1992] and the fractal dimension 'D' can differentiate between a'a ($D \leq 1.09$) and pahoehoe ($D \geq 1.15$) flows [e.g., *Bruno et al.*, 1994; *Baloga and Glaze*, 2003; *Crown and Baloga*, 1999; *Swanson*, 1973; *Kilburn and Lopes*, 1991]. Debris flows and pyroclastic flows can be differentiated from basaltic lava flows using this metric [*Michaels and Greeley*, 1996]. An impact melt flow might be expected to fall within the fractal range for lavas, with a lower D value than a dry granular flow.

LROC NAC images of a selection of dry granular, established impact melt flows, and ejecta flows from various lunar craters were analyzed in ArcMap (See Figure S1). The flow lobes were outlined as a series of points. The separation of these points (rod length, r) and distance along the flow lobe was then calculated. The distance between points was estimated with a linear 'rod'. We then used the "divider method" [c.f. Andrle, 1992] to calculate how the apparent length of the flow outline (L) changes when measured with virtual rods of different lengths (r). Here flow length $L = Nr$, where N is the number of rods. By plotting log L vs log r [c.f., *Richardson*, 1961], the fractal behavior can be determined. These measurements are plotted as in Supplemental Figure S2. We limited our fractal analysis to just a few large flows for two reasons: Firstly, most of the mapped flows around Pierazzo are observed near the limit of resolution, and so would provide an artificially smooth flow lobe for measurement rather than allowing a full analysis of the actual flow margin shape. Secondly, a diagnostic range of fractal dimensions for lunar impact melt flows has not yet been established for comparison. This work presents some of the first lunar melt and ejecta flow data points for this analysis.

3. Results

3.1 Pierazzo Mapping and Flow Morphology Results

Figure 2B shows the location of smooth low albedo deposits (light grey) and small-scale flows (black) identified around Pierazzo crater. The low albedo deposits have a smooth surface appearance relative to the surrounding area and can include features indicative of the presence of melt (e.g. fracturing, ponding in topographic lows, Figure 1B). Dark 'streamers' of material are noted in the near-rim region (e.g., Figure 3A). The streamers are comprised of low-albedo boulders (up to 80 m wide) that extend in discontinuous streaks up to 6 km from the rim and appear to lie on top of the generally lighter-toned continuous ejecta blanket. The boulders themselves might be light-toned blocks with a darker covering. These streamers remain within the areal extent of the continuous ejecta blanket which ends at an average distance of ~7km from the rim, slightly smaller than expected for an ejecta blanket around a crater of this size (c.f. *Melosh* [1989]). It is possible that streamers in this location continue beyond this distance, but are less visible due to lack of albedo contrast. Typical melt morphologies — ponds, flows and channels (e.g. Figure 3B) — are noted at the crater rim, particularly on the north and northwest sides. Flow lobes are more common than channelized flows and extend up to 2 km from near-rim ponds.

The first obvious flow features not associated with the crater rim melt ponds are noted at 1.6 km from the crater rim (0.35 crater radii). The example shown in Figure 4 is located on a crater-facing slope 11 km (2.5 crater radii) from the crater rim, within the discontinuous ejecta blanket. Approximately 140 similar flow features are found throughout the study area, up to a distance of ~40 km (~9 crater radii) from the crater rim (the maximum distance contained within the mosaic). Although numerous, each flow is small, resulting in a cumulative area for all the flows of ~50km^2. These features were identified as flows due to having distinct boundaries relative to the ejecta blanket around them. Flows can originate in amphitheater-headed depressions (e.g. Figures 1C, 4A), or occur without any obvious starting point to the flow (e.g. Figure 5A). Most, but not all, flows have relatively low albedo relative to surrounding ejecta in high sun images (e.g. Figure 4B). The largest flows in the mapping area display melt-like morphology more clearly than smaller flows (e.g. Figure 5). Smaller flows have hints of such morphology (Figure 6B), but this cannot be confirmed in all cases as these subtle surface texture can be ambiguous when viewed at the limit of image resolution. The length of flow can be up to 2.56 km, similar in size to the "splatter flows" noted within the continuous ejecta blanket of Aristarchus [*Zanetti*, 2015].

Pierazzo crater is located in the lunar highlands, which provides variable local topography that is lowest to the northwest and highest in the southeast (Figure 7). The topographic variance has allowed assessment of the role of surrounding topography on ejected melt emplacement. All flows in the mapping area occur on relatively shallow slopes, generally from 6 to 16°, but up to 18° in one location. Two thirds (67%) of the flows mapped within the extended ejecta blanket occur on crater facing slopes and flow back toward the crater (e.g. Figure 7). The other 33% of flows within the discontinuous ejecta tend to originate from various topographic obstacles such as pre-existing impact craters and then flow downslope regardless of orientation with respect to Pierazzo crater (e.g., Figure 6B). Flows with more muted morphology (lack of clear lobes) do occur without the presence of topographic obstacles (e.g. Figure S3). In these cases, the flows tend to be more linear, following the general path of the ejecta run-out. These features were not included in our dataset, unless they showed at least one flow lobe/toe, as they were deemed too similar to the surrounding ejecta to be noted as defined flows.

3.2. Supporting Fractal Analysis

We digitized the flow margins of 3 dry granular flows, 4 clear impact melt flows from various lunar craters and 7 distal ejecta flows from Giordano Bruno and Pierazzo (Figure S1). The length around each flow margin (L) was divided into 'rods' of differing lengths. The rod length (r) and number of rods (N = L/r) are plotted as Figure S1. All flows included in this analysis are fractal (Figure S2 shows straight lines in the log-log plot).

Figure 8 displays the fractal dimensions derived from this analysis. All confirmed (by the presence of characteristic melt textures) impact melt flows plot within the observed range, and slightly below that for basaltic terrestrial lava (~1.05–1.20; e.g., *Bruno et al*., 1994; *Schaefer et al.*, 2017). The lunar granular flows have D values outside of the range expected for lava flows (~1.30–1.35). The putative ejected melt flows presented in this work have fractal dimensions between 1.09 and 1.17, plotting over a similar D range as the established impact melt flows and the range expected for lavas.

4. Discussion

4.1. What is the nature of small-scale flows in the extended ejecta blanket of Pierazzo?

Flows and ponds with clear melt characteristics are mapped throughout the discontinuous ejecta blanket of Pierazzo crater. This includes the presence of wrinkling, cracking, channeling, ponding to an equipotential surface in topographic lows, and a generally lower albedo than the terrain around the flow (e.g., Figures 4–6). Deeper ponds and thicker flows tend to display more channeling, wrinkling and have a more notable albedo contrast to their adjacent terrain than the margins of these deposits, or smaller flows closer to the limit of resolution. Smaller flows that display similar broad morphology (lobate toes and clear flow paths) are possibly melt rich, but image resolution prevents the identification of cracks, wrinkling and channeling with certainty (e.g. Figure 6B). The origin point of these flows is obvious in some cases — an amphitheater-headed depression within the ejecta blanket (e.g., Figures 1C, 4A) which suggests the flow material came from within the ejecta mass itself (both rocky debris and melt) rather than being deposited on top of the ejecta. However, most flows have less defined starting points, possibly due to burial by still mobile ejecta around the flow initiation point.

All flows in the mapping area occur on relatively shallow slopes, generally from 6 to 16°, but up to 18° in one location. These slopes are too shallow for dry granular flows of angular grains beginning at rest [>23–30°, *Bagnold*, 1941; Pouliquen, 1999]. Within the energetic environment of impact ejecta emplacement, it could be argued that mobilization of dry debris might occur on slopes shallower than expected for the initiation of a granular flow at rest. However, the formation of these flows predominately on crater-facing slopes, and other locations in which the ejecta movement away from the crater has been impeded, suggests that most of these flows do form from an ejecta mass with a horizontal velocity of zero — inconsistent with a dry granular flow.

Fractal analysis of the margins of some of the flows also suggests that they are melt-rich as their fractal dimensions are similar to that recorded for impact melt and terrestrial lava flows, but very different from that expected for dry granular flows (Figure 8). This numerical analysis, combined with the melt-like morphology noted for the larger examples of these flows leads us to suggest that these features discovered within the extended ejecta blanket of Pierazzo are impact melt-rich flows.

Suspected ejected melt has also been noted in the high-resolution mapping of *Zanetti* [2015] and Kruger et al. [2016] within the Aristarchus and Tycho continuous ejecta blankets. Plescia [Pers. Comm., 2016] and work by this research team also notes melt deposits around several other lunar craters and extending at least 12 km from the rim of Giordano Bruno crater. Consequently, it is clear that melt deposits are a natural feature of ejecta blankets, but are only just being revealed by high-resolution studies of non-terrestrial craters for which the discontinuous ejecta is preserved. In the case of Giordano Bruno, the extended ejecta blanket covers a formidable lunar surface area. Our more manageable study area around the 9 km Pierazzo crater has enabled us to study the occurrence of this impact melt morphology within the majority of a discontinuous ejecta blanket within 9 crater radii from the crater center.

4.2. How can still-molten ejecta reach these distances?

Any possible melt flows in the extended ejecta blanket were determined as melt-rich, or not, on the basis of their morphology when compared to established melt flows such as those shown in parts of Figures 1 and S1. To then check if melt deposition at these locations within the ejecta blanket is physically possible, we estimated the cooling that would occur to melt within ejecta as it travels ballistically to such distances.

To simplify the situation, we assumed that impact melt at liquidus temperature is ejected in the form of spherical masses from the crater cavity, and these masses are cooled during their ballistic flight due to black-body radiation from their surface [e.g., *Yanagisawa and Kisaichi* 2002]. We employed standard data for silicate rocks (heat of fusion $L=4.2\cdot10^5$ J/kg, liquidus-solidus temperatures, T_l= 1450 K, T_s= 1270 K, respectively) and an efficient heat capacity value between solidus-liquidus $C=C_0+L/(T_l-T_s)$ [*Onorato et al*., 1978]. For the flows investigated in this manner, the ballistic flight time of ejecta to reach the flow location was estimated based on ballistic equations, combined with ejecta scaling laws [*Housen and Holsapple*, 2011]. Our model likely overestimates the cooling rate (and, hence, underestimates the melt fraction in arriving ejecta) as molten blobs within a dense (and optically thick) ejecta curtain cool slower (they not only emit radiation, but also absorb radiation from nearby hot fragments).

The origin (marked X) of the flow in Figure 4A is 11 km away from the crater rim and appears to break out from within the ejecta deposit and flow toward the crater down a slope of ~15° for 1.2 km indicating good mobility. The ballistic equations, combined with ejecta scaling laws [*Housen and Holsapple*, 2011], suggest that at a distance of 11 km from the crater we would expect ejected material to strike the ground ~2 minutes after ejection, arriving with a speed of ~130 m/s. For the more remote flows at the edges of the mapping area (distance ~45km from the crater center) we predict an ejecta impact speed of 270 m/s, arriving approximately 4 minutes after ejection from the parent crater.

Area measurement from NAC imagery and flow thickness estimates from shadow-lengths suggest a flow volume of ~10^5 m^3 for the western-most flow in Figure 4A. Using the thermal model presented in Section 2.3, we found that after four minutes in flight 1-cm-diameter particles are totally solidified; 60% (by mass) of 10-cm-diameter particles are still above the solidus; and meter-sized blobs have only a thin solid shell whereas 97% of their mass is still molten. It is therefore not surprising that a flow of 10^5 m^3, if impact melt-rich, can still demonstrate a high degree of melt mobility after flight.

4.3. Why are melt flows formed in the observed locations?

Our mapping reveals that 1.5% of the area of study area contains ejecta with clear melt flow morphology in the extended ejecta deposit. Even with high-resolution mapping, it is curious that isolated flows are not more common within ejecta deposits. Our results show that two thirds of the mapped flows occur on crater-facing slopes (e.g., Figure 7). The other third of the mapped flows emerge from pre-existing topographic lows (e.g. Figure 6B). We present a possible explanation for concentration of these melt deposits around Pierazzo primarily on crater-facing slopes in Figure 9. A ground-based flow at the speeds estimated for these deposits will be highly turbulent and have a Froude number of order 10^2, well in excess of anything commonly seen on earth, and will rapidly entrain surface debris [e.g., *Oberbeck*, 1975]. Both are factors that will lead to the rapid cooling of most entrained impact melt within that ground flow (Figure 9A). The development of melt-like morphology (flows) of these melt-rich ejecta deposits therefore requires an additional factor. We suggest that the presence of a topographic obstacle or crater-facing slope facilitates the formation of melt flows by impeding the ejecta mass soon after it makes ground contact. This prevents vigorous mixing of the solid and molten debris, allowing the melt to separate out from the ejecta deposit and flow out toward lower elevation. This hypothesis is depicted in Figure 9B.

Even without continued along-ground flow, some mixing of solid and molten debris will occur when the ejecta impacts the ground. We thus expect ejected melt flows to form only in cases where the melt content of the ejecta was particularly high in that region. If melt content in the ejecta is high enough, the additional mobility created due to the pre-existing topographic slope could allow the melt to escape the mixture and form flows. Figure 9 depicts a simplified scenario in which a single large pocket of melt extrudes from a stalled ejecta flow. It should be noted that, for larger craters than Pierazzo, the greater amount of melt produced could allow for formation of ejecta melt flows among the extended ejecta blanket without the need for the interference of topography (e.g. Figure S3).

Our presented model concerns the formation of clear (lobed toes, defined margins relative to the surroundings) flows within the ejecta that originate from crater-facing slopes or topographic obstacles. However, our hypothesis does not consider more linear flows without toes/lobes (e.g. Figure S3) that occur without the presence of topographic obstacles around Pierazzo and other lunar craters. These flows lack clear toes/lobes and tend to follow the general path of the ejecta. These were not included in our data set, but could represent a continuum morphology between the defined flows (e.g. Figure 5) and the main body of the ejecta blanket. In these cases, it is possible that these ejecta features are also melt-rich (based on the similar mid-flow morphology). It is possible that the melt content of the ejecta was particularly high in this region, allowing muted melt-morphology to form without the complete stall of the ejecta flow.

Although some large (~10–100m) melt rock outcrops have been noted on top of the near-rim ejecta of the Ries crater [e.g., *Stöffler et al.,* 2013], evidence for large melt deposits on, or in, the ejecta blankets of terrestrial craters is sparse (perhaps because preserved ejecta blankets on Earth are themselves rare [*Osinski et al.,* 2011]). Smaller globules of melt that are better mixed with solid debris are statistically more likely, and more supported by the terrestrial literature. Surficial flow formation might still occur in these cases if the melt can filter out of a solid debris deposit of sufficient porosity. Modeling work to determine the size of melt pockets and the porosity of solid ejecta that would allow for flow formation is underway, but is beyond the scope of this paper.

4. Conclusions

We have identified distinct flow features throughout the extended ejecta blanket of Pierazzo crater, reaching at least 40 km from the crater rim. Two thirds of these flows occur on crater facing slopes and flow downhill, suggesting that these flows started without the original forward momentum of the ejecta curtain. The 140 flows included in our mapping area occur on slopes of 6 to 18° — too shallow for the formation of granular flows from rest with angular grains. These shallow slopes, combined with clear melt morphology observed on the largest flows and ponds, suggest that these flows are impact melt-rich. This result is supported by fractal dimensions for the flow boundaries of D = 1.05–1.17. These values are consistent with terrestrial basaltic lava flows (D = 1.06–1.2) and established lunar impact melt flows (D = 1.06–1.18), but inconsistent with lunar dry granular flows (D = 1.31–1.34). Our results suggest that impact melt is incorporated into the ejecta and emplaced ballistically (with some subsequent ground flow). This supports the idea that impact melt can travel far from the host crater.

Although our results show that the extended ejecta blanket of Pierazzo crater contains numerous possible melt deposits, the area of these flows make up only 1.5% of our mapping area. As the presence of impact melt in ejecta blankets on Earth is well established (in the ground mass, but not as defined flows. e.g., *Stoeffler et al.,* 2013; *Osinski et al*., 2015), this low areal percentage suggests that most ejected melt from a crater of the size of Pierazzo (D = 9 km) remains entrained with solid ejecta. We suggest that most ejecta impacts the ground and continues to travel across the surrounding terrain at speeds high enough to maintain turbulence in the flow, preventing any coherent melt pockets from settling out, and further mixing them with the solid debris.

Two-thirds of the flows mapped in this work occur on crater-facing slopes, suggesting that the likelihood of actual melt flows developing within the ejecta deposit is increased by the presence of high crater-facing topography (e.g. Figure 7), or a defined topographic low (e.g., Figure 6), to stall or impede the ejecta flow soon after it makes ground contact, limiting turbulent mixing. We hypothesize that impact melt flows will form from a 'stalled' ejecta in cases where a) the melt content of the ejecta is particularly high, b) the size of melt pockets within the ejecta deposit is large, and/or c) the porosity of the solid ejecta is notable enough to allow melt from multiple melt pockets to drain out before solidifying (e.g. Figure 9). Formation of flow morphology then depends upon the local topography.

Acknowledgments

We wish to acknowledge the Lunar Reconnaissance Orbiter LROC team for acquiring and processing the data presented here, and to our two reviewers: Jeff Plescia and Gordon Osinski. Data from the LRO mission is made publicly available through the Planetary Data System (pds.nasa.gov). This work was supported by the LRO project and by NASA Lunar Data Analysis Program Grant NNX15AP93G.

References

Andrle, R. (1992) Estimating fractal dimension with the divider method in geomorphology. Geomorphology 5(1-2): 131-141.

Artemieva, N. (2013), Tycho Crater Ejecta, Lunar and Planetary Science Conference, abstract No. 1719, p. 1413.

Bagnold, R.A. (1941): The physics of blown sand and desert dunes. London: Methuen". *Progress in Physical Geography*. **18** (1): 91. doi:10.1177/030913339401800105.

Bandfield, J. L., J. T.S. Cahill, L.M. Carter, C. D. Neish, G.W. Patterson, J-P Williams and D. A. Paige (2016), Distal ejecta from lunar impacts: Extensive regions of rocky deposits. Icarus, In Press.

Bray, V. J., L. L. Tornabene, L. P. Keszthelyi, A. S. McEwen, B. R. Hawke, T. A. Giguere, S. A. Kattenhorn, W. B. Garry, B. Rizk, C. M. Caudill, L. R. Gaddis, and C. H. van der Bogert (2010), New insight into lunar impact melt mobility from the LRO camera, Geophysical Research Letters, 37, doi:10.1029/2010GL044666.

Bruno, B.C., G. J. Taylor, S. K. Rowland, et al. (1994). Quantifying the effect of rheology on lava-flow margins using fractal geometry. Bulletin of Volcanology 56: 193. doi:10.1007/BF00279604.

Bruno B. C. , G. J. Taylor, S.K. Rowland, P.G. Lucey, S. Self (1992) Lava flows are fractals. Geophysical Research Letters 19: 305–308.

Bruno B. C., G. J. Taylor, S.K. Rowland, S.M. Baloga (1994) Quantifying the effect of rheology on lava-flow margins using fractal geometry. Bulletin of Volcanology 56:193–206.

Carter, L. M., C. D. Neish, D. B. J. Bussey, P. D. Spudis, G. W. Patterson, J. T. S. Cahill, and R. K. Raney (2012), Initial observations of lunar impact melts and ejecta flows with the Mini-RF radar, *Journal of Geophysical Research*, *117*, doi:10.1029/2011JE003911.

Chadwick, D. J. and G. G. Schaber (1993), Impact crater outflows on Venus: Morphology and emplacement mechanism. Journal of Geophysical Research 98(E11):20891-20902.

Crown, D. and S. Baloga (1999), Pahoehoe toe dimensions, morphology, and branching relationships at Mauna Ulu, Kilauea Volcano, Hawai'i. Bulletin of Volcanology 61(5):288-305.

Dence, M. R., R.A.F. Grieve and P.B. Robertson [1977]. Terrestrial impact structures: principal characteristics and energy considerations. In D.J. Roddy, R. O. Pepin and R. B. Merrill (Eds.) Impact and Explosion Cratering, Pergamon Press, New York, pp. 247-275.

Hawke, B.R. and J.W. Head (1977), Impact melt in lunar crater interiors. In: D.J. Roddy, R.O. Pepin, and R.B. Merrill (Eds.), Impact and explosion cratering. Pergamon Press, New York, NY, pp. 815.

Housen, K. R., and Holsapple, K. A. (2011), Ejecta from impact craters, *Icarus, 211*, 856–875, doi:10.1016/j.icarus.2010.09.017.

Kilburn, C. R. J and M. C. Lopes (1991). General patterns of flow field growth: aa and blocky lavas. Journal of Geophysical Researzch 96(B12):19721-19732.

Kraus, R. G., L. E. Senft and S. T. Stewart (2011), Impacts onto H2O ice: Scaling laws for melting , vaporization, excavation and final crater size. Icarus 214:724-738.

Kruger, T., C. H. van der Bogert and H. Hiesinger (2016). Geomorphologic mapping of the lunar crater Tycho and its impact melt deposits. Icarus 273:164-181.

Maxwell, D., 1977. Simple Z model of cratering, ejection, and the overturned flap. In: Roddy, D., Pepin, R., Merrill, R. (Eds.), Impact and Explosion Cratering. Pergamon Press, New York, pp. 1003–1008.

Melosh, H.J. (1989) Impact cratering. Oxford University Press, Oxford, UK.

Michaels, G. and R. Greeley (1996), Lava, debris and pyroclastic flow deposits: analysis and identification using curvature spectra. Proceedings of LPSC XXV11, pp 877-878.

Neish, C. D., J. Madden, L. M. Carter, B. R. Hawke, T. Giguere, V. J. Bray, G. R. Osinski, J. T. S. Cahill (2014). Global distribution of lunar impact melt flows. Icarus 239:105-117.

Oberbeck, V. R. (1975), The role of ballistic erosion and sedimentation in lunar stratigraphy. Reviews of Geophysics, 13(2):337-362.

Onorato P.I.K., Uhlmann D. R., and Simonds C. H. 1978. The thermal history of the Manicouagan impact melt sheet, Quebec. *JGR* 83: 2789–2798.

Osinski, G. R., L. L. Tornabene, and R. A. F. Grieve (2011), Impact ejecta emplacement on terrestrial planets, Earth and Planetary Science Letters, 310, 167–181, doi:10.1016/j.epsl.2011.08.012.

Osinski, G. R., T. E. Bunch, R. L. Flemming, E. Buitenhuis and J. H. Wittke (2015). Impact melt- and projectile-bearing ejecta at Barringer Crater, Arizona. Earth and Planetary Science Letters 432:283-292.

Pike, R. J. (1976), Crater dimensions from Apollo data and supplemental sources, The Moon, 15, 463-477.

Plescia, J. B., and M. J. Cintala (2012), Impact melt in small lunar highland craters, Journal of Geophysical Research, 117, doi:10.1029/2011JE003941.

Plescia, J. B. (2015), Lunar Crater Forms on Melt Sheets — Origins and Implications for Self-Secondary Cratering and Chronology, Lunar and Planetary Science Conference, 46, 2054.

Pouliquen, O. (1999), Scaling laws in granular flows down rough inclined planes, Physics of Fluids, 11, p. 542–548, doi: 10.1063/1.869928.

Robinson, M.S., and 22 colleagues (2010), Lunar Reconnaissance Orbiter Camera (LROC) instrument overview, Space Science Reviews, 150, 81-124, doi:10.1007/s11214-010-9634-2.

Robinson, M. S. and 11 colleagues (2016), An exceptional grouping of lunar highlands smooth plains: Geography, morphology and possible origins. Icarus 273:121-134.

Schaefer E. I., C. W. Hamilton, C. D. Neish, M. M. Sori, A. M. Bramson, S. P. Beard, S. I. Peters, T. A. Miller, and E. L. Rader (2017), Seeing pahoehoe from orbit (without squinting), Lunar and Planetary Science Conference abstract No. 1964

Scholten, F. J. Oberst, K.-D. Matz, T. Roatsch, M. Wahlisch, E. J. Speyerer, M. S. Robinson (2012). GLD100: The near-global lunar 100m raster DTM from LROC WAC stereo image data. Journal of Geophysical Research Vol. 117 DOI: 10.1029/2011JE003926.

Stöffler, D. and Grieve, R. A. F. (2007) Impactites, Chapter 2.11 in Fettes, D. and Desmons, J. (eds.) Metamorphic Rocks: A Classification and Glossary of Terms, Recommendations of the International Union of Geological Sciences, Cambridge University Press, Cambridge, UK, 82-92, 111-125, and 126-242

Stoeffler, D., N. A. Artemieva, K. Wunnemann, W. U. Reimold, J. Jacob, B. K. Hansen and I. A. T. Summerson (2013). Reis crater and suevite revisited – Observations and modeling Part I: Observations. Meteoritics and Planetary Science, 48(4):515-589.

Stopar, J. D., B. R. Hawke, M. S. Robinson, B. W. Denevi, T. A. Giguere, and S. D. Koeber (2014), Occurrence and mechanisms of impact melt emplacement at small lunar craters, Icarus, 243, 337–357, doi:10.1016/j.icarus.2014.08.011.

Swanson, D. A., Pahoehoe flows from the 1969 – 1971 Mauna Ulu eruption of Kilauea volcano, Hawaii, Geol. Soc. Am. Bull., 84, 615 – 626, 1973

Yanagisawa M and Kisaichi N. (2002), Lightcurves of 1999 Leonid Impact Flashes on the Moon. *Icarus* 159: 31-38.

Zanetti, M. R. (2015). Investigating the complexity of impact crater ejecta. PhD thesis for Washington University, St. Louis. pp 218.

Zanetti, M., A. Stadermann, B. Jolliff, H. Hiesinger, C. H. van der Bogert and J. Plescia (2017). Evidence for self-secondary cratering of Copernican-age continuous ejecta deposits on the Moon. Icarus, In Press.

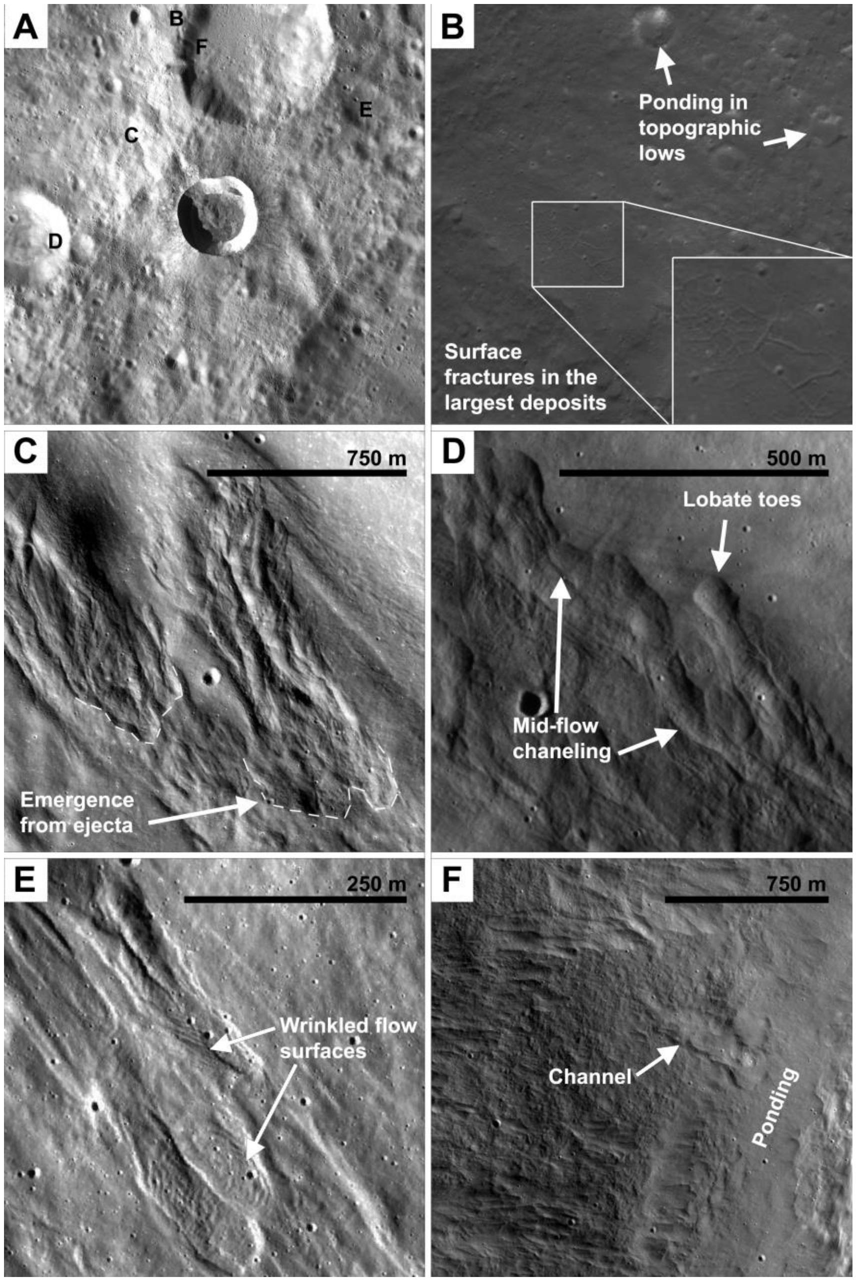

Figure 1: Examples of impact melt morphology. North is up in all images. A) Context image for the 22km diameter Giordano Bruno lunar crater. Locations of the close-up images shown in sections B-F are marked. B) Ponds of low albedo melt approximately 52 km from the crater rim. The melt ponds into pre-existing topographic lows. Inset is ~250 m across and shows cracking in a particularly deep pond. LROC image M141586559. C) Possible melt-rich flows emerging from the ejecta blanket and flowing downhill (M1098172472). D) General flow lobe shape and channelization (M1095821669). E) Wrinkled surfaces of a melt flow approximately 35 km northwest of Giordano Bruno (M165170213). F) Flows similar to the complex flow shown in C, flowing downhill and connecting with ponds of impact melt. This physical connection suggests that these flows, and perhaps that in Figure 1C, are or were melt-rich.

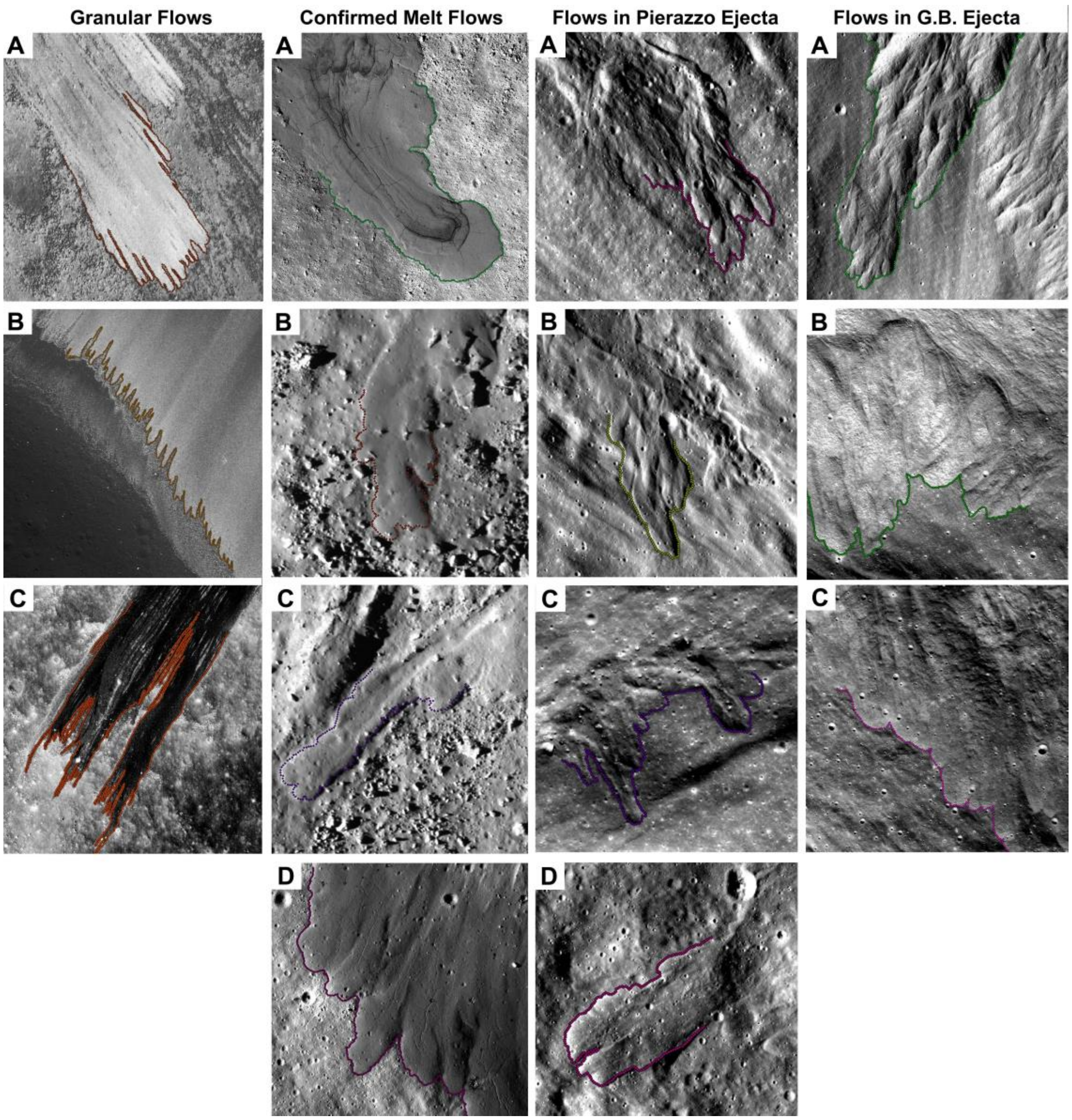

Figure S1: Outlining different flows for fractal analysis. Column 1 shows granular flows, identified as such due to their granular appearance at high resolution and the lack of ponding to an equipotential surface in topographic lows. A and B) Bright granular flows on the wall of Adams crater, M141839028L C) Dark granular flow on the interior wall of a crater that formed on the eastern wall of Virtanen crater. M169398317L. Column 2: Established impact melt flows. A) Impact melt flow extending from the south-west rim of Giordano Bruno crater, M152207959L. B and C) Channeled and lobate flows Byrgius A, M1169949846R and M193367401R. D) A 1km section of the ~ 18 km flow emanating from the disrupted southern rim of Korolev X, MM1143447837. Column 3: Flows mapped in the discontinuous ejecta blanket of Pierazzo crater as part of this work. A and B) See Figure 4, M166501049R and M166507836R. C) See Figure 5, M112251205R. D) A flow West of Pierazzo, M114620473L, see Figure 2A for position. Column 4: Flows mapped within the discontinuous ejecta of Giordano Bruno crater that are suspected to be melt-rich, but have not been confirmed by the identification of the typical melt characteristics described above. LROC NAC M161646501L.

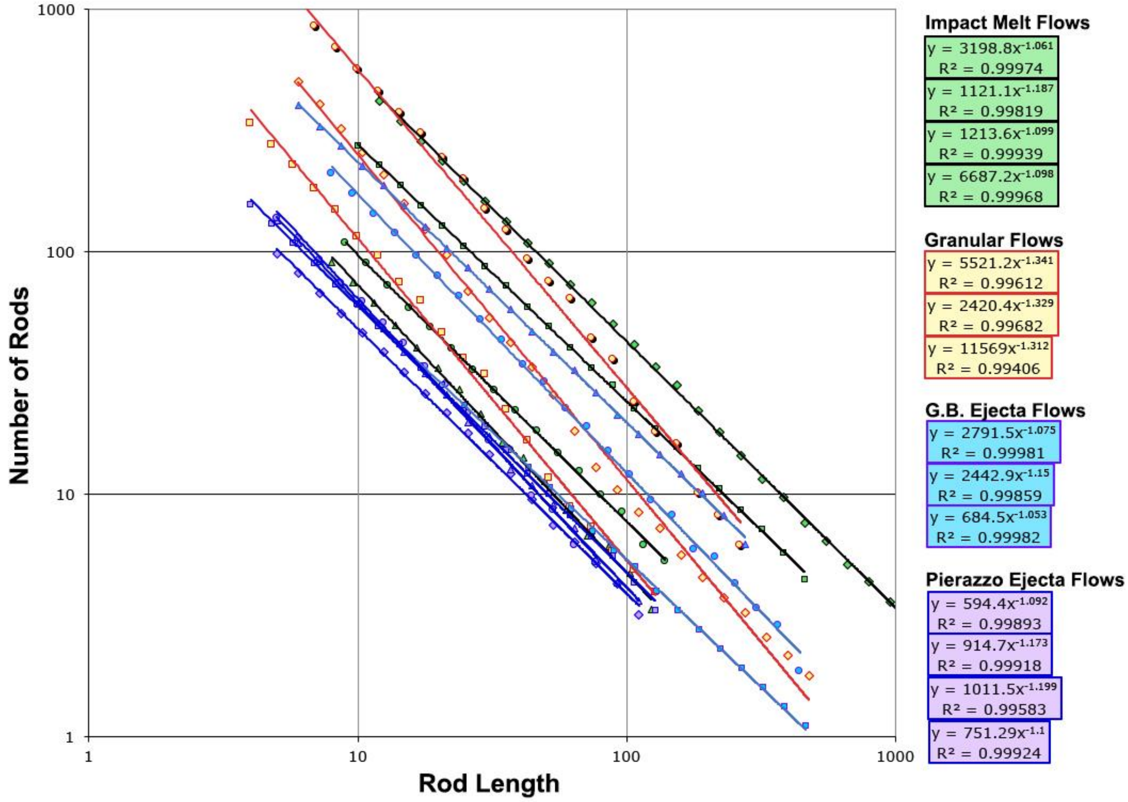

Figure S2: Fractal dimensions of flow margins mapped in this work (See Figure S1 for images of the point locations). If the trend is linear in this log plot then it indicates that the flow margin is fractal. The fractal dimension can then be extracted from the trend line equation.

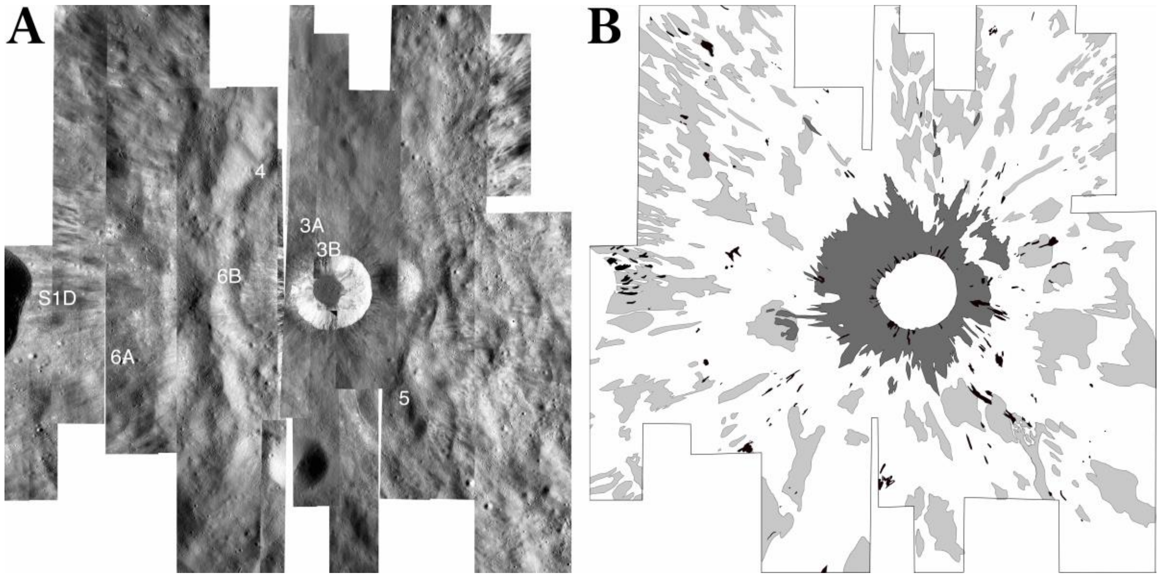

Figure 2: A) LRO NAC mosaic of the Pierazzo crater and surrounding area. The mosaic resolution was normalized to 1.5 m. North is up. White text denotes the location of the different flows featured in other figures. B) Map of possible ejected melt, where black = suggested melt flows, dark grey = blocky low albedo ejecta that includes ‘streamers’, light grey = regions of low-albedo candidate melt deposits. This latter group commonly had more melt-like texture than the surrounding rubbly ejecta deposit such as lobate edges and ponding to equipotential surfaces in topographic lows.

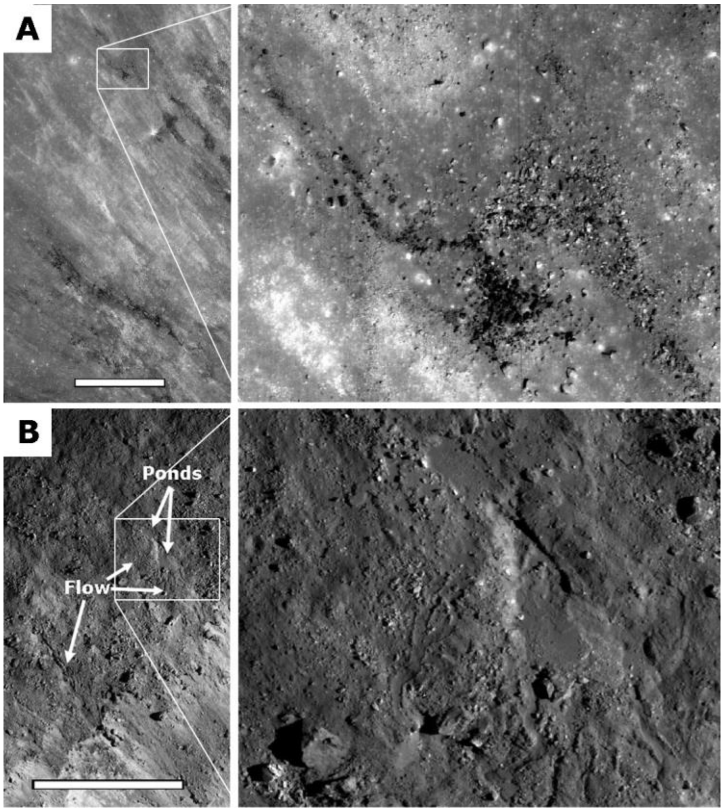

Figure 3: (A) Example of dark streamers observed in the near-rim region. Scale bar is 1 km. Close-up shows their blocky texture. LROC NAC M109895309. (B) Impact melt flow associated with ponds located near the crater rim. Ponds are at the top of the close-up, flows are at the bottom of the close-up image. LROC NAC M160607763. Scale bar is 1 km. North is up and Pierazzo crater lies to the bottom right in both images. For locations of these images, please see Figure 2A.

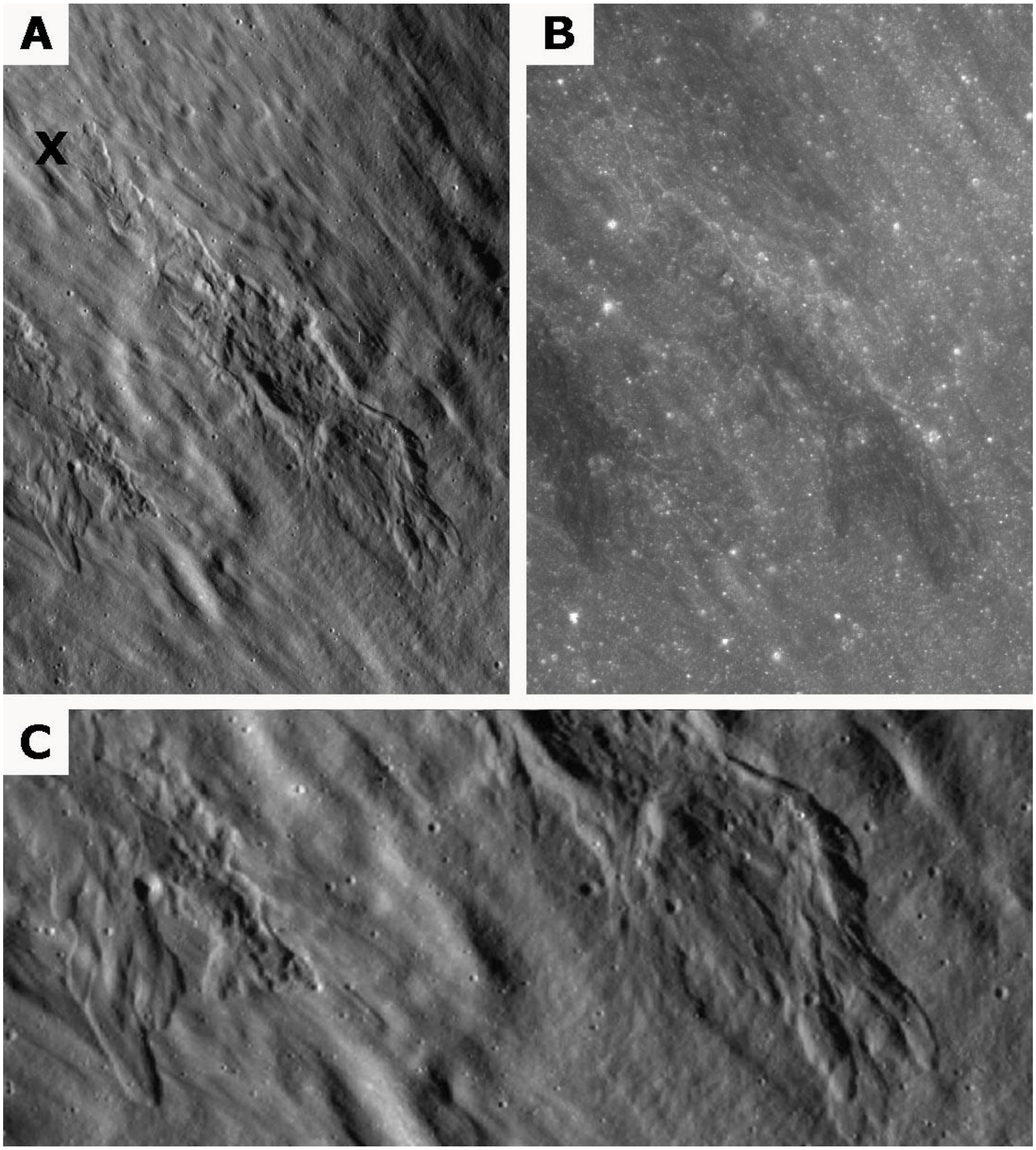

Figure 4: Two flows noted 11km (2.5 crater radii) from the rim of Pierazzo, within the craters discontinuous ejecta blanket. In all images: North is up, Pierazzo is to the southeast, and downhill is to the bottom right. A) LROC image M102816150 of the full flow, including the point at which the flow appears to emerge from the ejecta deposit (X). B) High sun image (M109895309) demonstrating the low albedo of this deposit relative to the surrounding ejecta. C) A close up of the flow toes. This image is 1 km across.

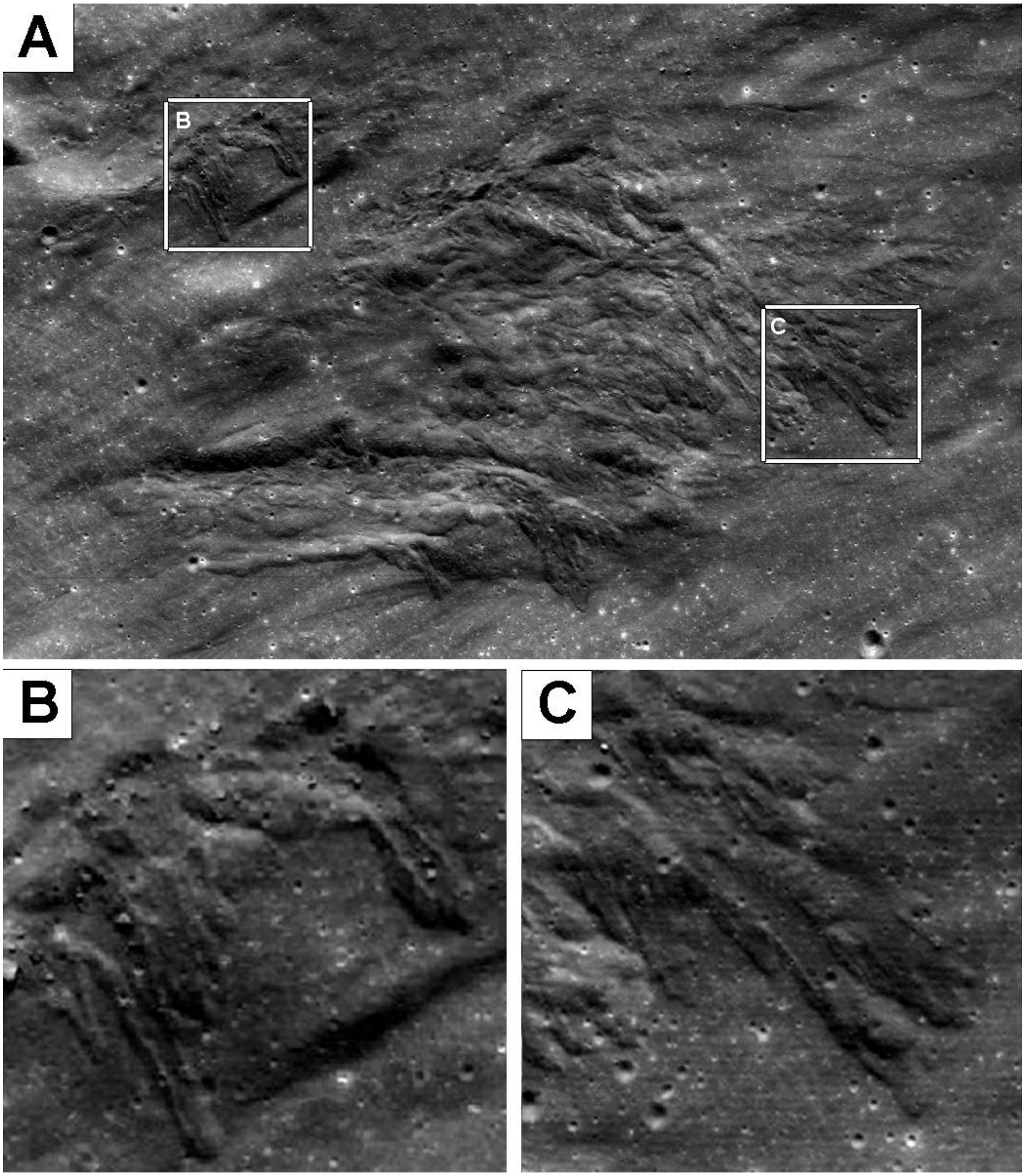

Figure 5: A ~ 1.5 km long complex flow within the discontinuous ejecta blanket southeast of Pierazzo. North is to the left. Downslope is to the bottom right. Close ups of the flow toes are shown in B and C. These examples show the formation of channels due to the drainage of melt from within cooled outer margins of these flow lobes. LROC image M11225120.

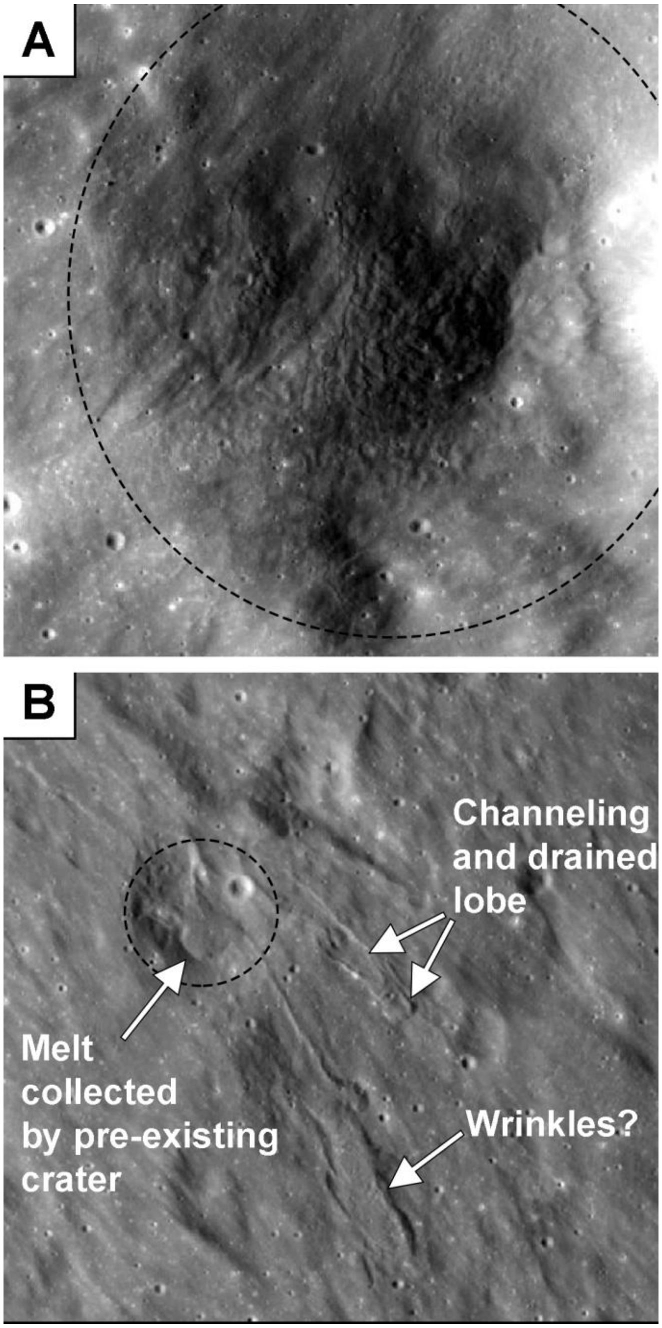

Figure 6: LRO NAC images of ejected melt pooling in and flowing from pre-existing craters (dotted black circles) around Pierazzo crater. North is up in both images, each image is 750m across.. A) Wrinkled/fractured surface texture is observable in this example, perhaps because the pre-existing crater enabled a relatively deep deposit to collect. B) Flows from a ponded melt deposit in a pre-existing crater.

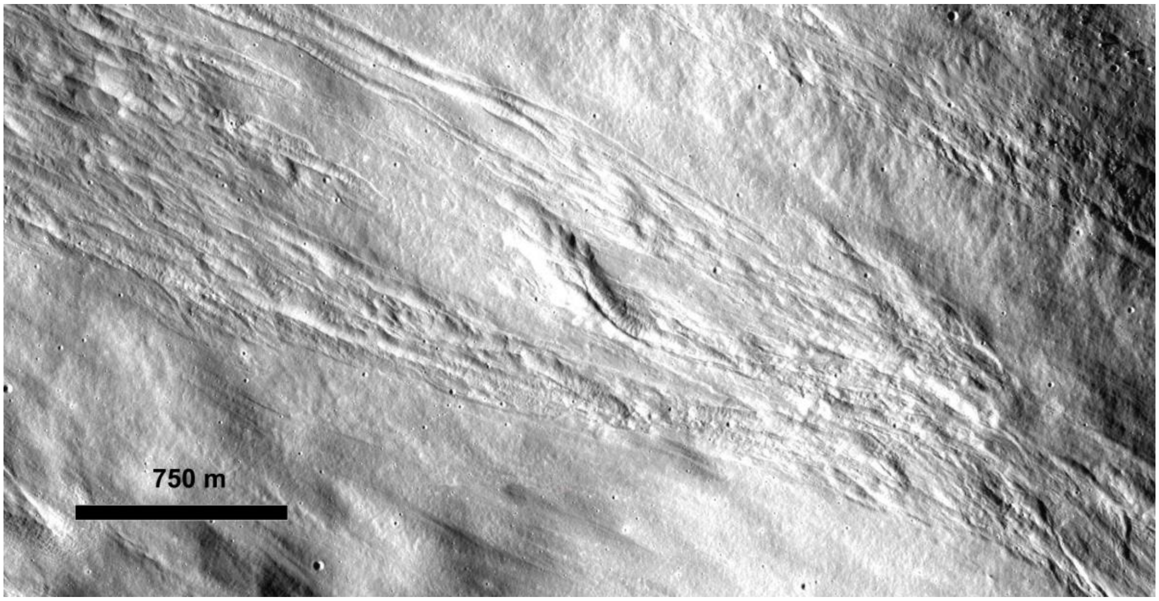

Figure S3: These ejecta streaks have surface texture similar to the mid-flow mottling of our mapped flows, but lack clear toes/lobes and tend to follow the general path of the ejecta. As a result, these types of flows/streaks were not included in our flow mapping. The location of this ejecta streak around Giordano Bruno crater is noted in Figure 2. North is up, Giordano Bruno lies to the bottom right of the image and downhill (on a 15 degree slope) is to the upper left. These types of features do not require crater-facing slopes to form and might be examples of locations where the ejecta was particularly melt rich. If this is a melt-related morphology, then these streaks represent an intermediate morphology between the melt flows and rocky ejecta of the distal ejecta blanket.

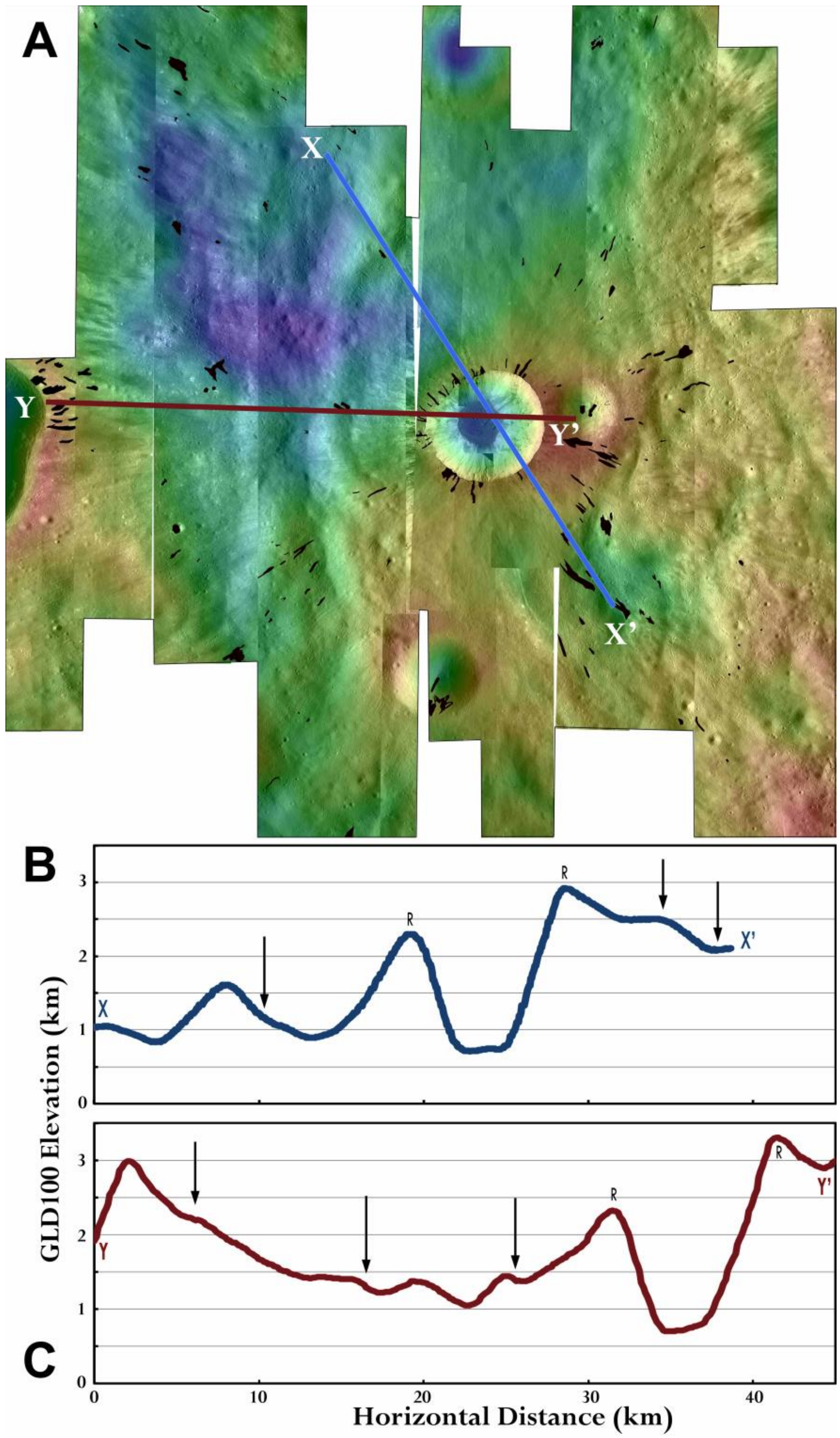

Figure 7: A) GLD100 topography of the study region, with the location of impact melt flows marked in black. These include near-rim flows and those noted within the areal extent of the ejecta. B and C) Topographic profiles through the crater. Locations of impact melt flows are indicated by arrows, and the crater rim is marked by the letter 'R'. The large flow pictured in Figure 4 is shown with the farthest left arrow in the topographic profile shown in B.

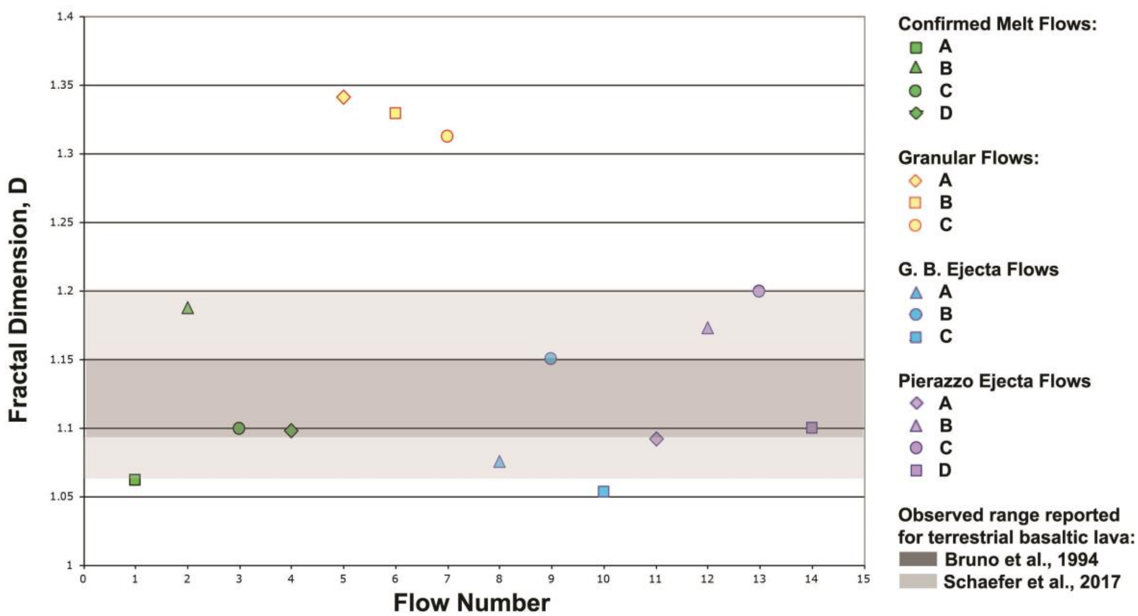

Figure 8: Fractal dimensions (D) of various flows. Images of each flow are shown as Figure S1. The span of D values noted for terrestrial basalt lavas is shaded grey. Note that *Schaefer et al*. [2017] computed a larger range of D values, because they included rubbly and slabby 'transitional' basaltic flows, in addition to the pahoehoe and a'a flows studied in *Bruno et al*. [1994]. All impact melt flows and the putative ejected melt flows presented in this work plot within this range. The granular flows measured in this work have D values outside of the range expected for lavas.

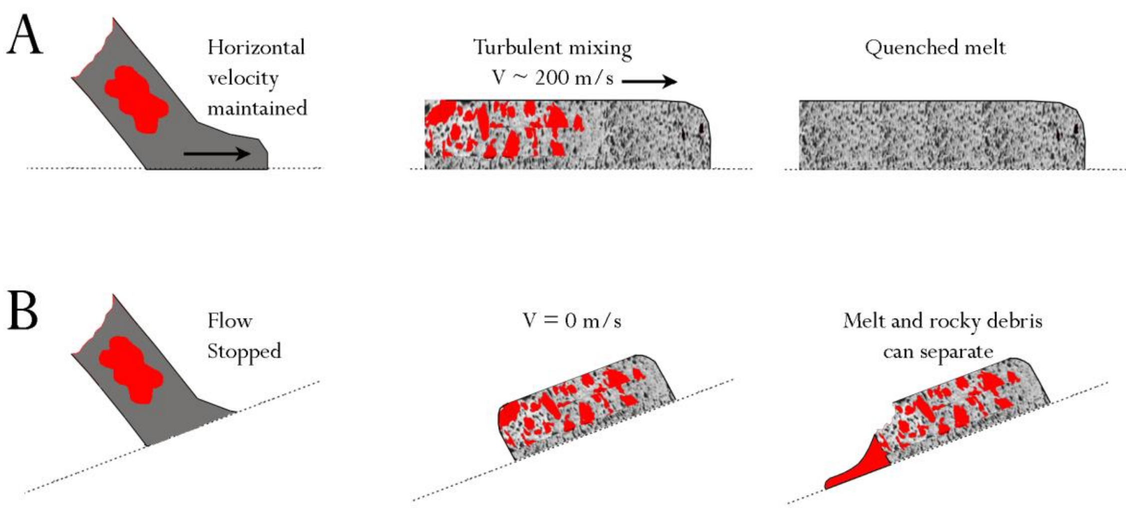

Figure 9: A) Ground flows will incorporate surface debris that rapidly quench any impact melt in the ejecta blanket. Such melt would not form flows, and would be difficult to identify through remote sensing. B) If a topographic obstacle stops the motion of the ejecta, this will inhibit any turbulent mixing of melt and debris, keeping the ballistically emplaced melt molten. At this point, the melt can separate out from the ejecta blanket and flow towards lower elevations. From our mapping, a crater-facing slope of 6-18° is sufficient.